# INVESTIGATION OF

# TRAVELLING IONOSPHERIC DISTURBANCES

Polytechnic Institute of New York

Subcontract 23719 under
NASA Grant NAGW-51

Final Report

For the period 1 March 1980 - 28 February 1981

Principal Investigator

Dr. Mario Grossi



March 1981

Prepared for

Polytechnic Institute of New York
Farmingdale, N.Y. 11735

Prepared for

Smithsonian Institution
Astrophysical Observatory
Cambridge, Massachusetts 02138

The Smithsonian Astrophysical Observatory
and the Harvard College Observatory
are members of the
Center for Astrophysics

## Foreword

This Final Report on PINY subcontract 23719 under NASA Grant NAGW-51 fulfills the obligations of the Smithsonian Astrophysical Observatory (SAO) for this contract.

The period of performance was March 1, 1980 to February 28, 1981. Dr. Mario D. Grossi was Principal Investigator, Dr. R.D. Estes served as Co-Investigator. Program Manager for this effort was Mr. Richard S. Taylor.

The Project generated an Interim Report for the period March 1, 1980 through September 30, 1980, delivered to PINY in early October 1980. In November 1980 SAO also submitted to PINY Proposal P-1046-11-80 for the continuation of the investigation for an additional year.

Professor Stanley H. Gross, Principal Investigator for NASA Grant NAGW-51, directed this effort for PINY.

## Abstract

We have reduced again and re-analyzed the Satellite-to-Satellite Doppler tracking data that were collected by SAO during the 1975 ASTP mission (Experiment MA-089) at an orbital altitude of about 220 km.

Maximum entropy power spectra of the ionospheric electron density were constructed to enable PINY to compare them with the power spectra independently obtained by PINY with in situ measurements of ionospheric electron density and neutral species performed with instrumentation carried by the Atmospheric Explorer (AE) satellite. This comparison was meant to provide corroborative evidence on the geophysical reality of the alleged electron density irregularities detected by the ASTP dual-frequency doppler link. In addition, the data were further analyzed at SAO to search for events of particular geophysical significance. The results can be summarized as follows.

The maximum entropy power spectrum of the electron density shows a peak corresponding to wavelengths of 250-300 km. A high-pass filtering of the data reveals localized regions of fluctuations in the electron density having amplitudes of 3 to 5 x $10^9$ $m^{-3}$ and wavelengths less than 300 km. Roughly half of the localized wave structures, which are confined to dimensions of 1800 km or less (as seen by an orbiting doppler baseline), are found to be associated with the larger crest of the geomagnetic anomaly in the southern (winter) hemisphere in the morning. The observed nighttime structures are also associated with local peaks in the electron density. We observe other wave structures at the day-to-night transition point, and we suggest atmospheric disturbances caused by the supersonic motion of the terminator as a possible generating mechanism. The amplitudes of the wave structures are roughly independent of the background density, in agreement with previous observations of Travelling Ionospheric Disturbance (TIDs). We conclude that our observations are consistent with medium-scale TIDs generated by atmospheric gravity waves.

## 1. Outline of the Investigation and Illustration of the Results

SAO performed the following data reduction and processing tasks during the contractual activity:

a) Verified the correctness of the time marks on the NAGRA ASTP doppler data records (data collected by the ASTP-MA-089 Experiment). This verification was done in two separate and independent ways, in order to increase the reliability of the determination. In addition, the required doppler information was extracted from the tapes, and orbital data were generated to be utilized in the data interpretation and analysis;

b) Obtained differential doppler data as a function of time, and correlated with satellite ephemerides (relation to electron density gradient shown in equations 1 through 6 of Appendix A);

c) Integrated differential doppler data to obtain electron density along satellite orbit (see Appendix A for discussion concerning integration constant);

d) Obtained power spectrum of electron density data, using maximum entropy method. Observed a distinct peak in the 220-320 km wavelength band;

e) Applied high-pass filter to the data and observed a number of wavepacket-like structures at intervals in the data (wavelength <300 km, train length about 1500-2000 km).

The data analysis tasks performed by SAO provide the following results:

A) A number of well-known ionospheric phenomena were clearly identified in the ASTP data. In particular, the Appleton or equatorial anomaly is evident in several different ASTP revolutions, with the relative size of the two crests in good agreement with independent observations for the same season and region. It should be noted that the magnetic equator indicated in the Figures of Appendix A refers to zero dip angle points rather than the to the less appropriate dipole equator used in earlier plots. The day-to-night variations in electron density are of the right magnitude and show dramatic changes at day/night transitions.

These observations, discussed more extensively in Appendix A, inspire confidence that we are indeed observing real ionospheric phenomena;

B) The hypothesis that the wave structures observed in the filtered data are medium-scale TIDs generated by atmospheric gravity waves is shown to be consistent with a number of previously observed characteristics of these phenomena, including location and local timing of the events, observed wavelengths, amplitude variations, etc.;

C) Assuming that the observed structures are indeed TIDs, the connection between TID and the sharper, winter hemispheric, morning crest of the equatorial anomaly appears to be a new observation. We submit that the steep vertical electron density gradient associated with these crests is probably the decisive factor in generating this phenomenon;

D) Another possibly significant observation is that of the very sharp spikes in electron density, accompanied by short-wavelength waves structures, seen in two ASTP revolutions at the day-to-night transition point. We suggest that this behavior resembles what one would expect at a shockwave front and note that shockwaves generated by supersonic terminator motion have been proposed as TID-generating mechanisms, but have never been directly observed in ionospheric data;

E) Nighttime wave structures seen in the ASTP data correlate well with previously-observed structures with regard to location and local time.

Concerning the comparison that had been initially planned between the ASTP data and vertical incidence ionograms from ground-based stations and from top-side sounders, we report that SAO procured from NOAA (World Data Center A) ionograms from 15 ground-based stations and additional reels of tape from top-side sounders. However, a review of these records disclosed that because of sounders' outages, there was not a single temporal and spatial coincidence between the NOAA-WDC-A data and the ASTP data.

We had to search, therefore, for evidence of a corroborative nature in the AE data collected by PINY. Qualitatively speaking, a remarkable similarity is already becoming evident between the power spectra of the density of neutral nitrogen, atomic oxygen and electrons obtained by the AE satellite and the ASTP MA-089 observations.

The SAO analytical effort centered on the geophysical interpretations of the phenomena seen in the data. This involved literature searches, verification that well-known ionospheric phenomena are seen in the data, and refinement of the analytical approach. The results of this investigation are reported in detail in Appendix A. Appendix A is a substantially modified version of Appendix I of the SAO Interim Report to PINY, with greatly augmented geophysical interpretation. We plan to submit a paper to a suitable journal, such as Radio Science based on the content of Appendix A. We also plan to prepare a joint paper with PINY, by combining AE observations and ASTP observations.

## 2. Conclusions and Recommendations

Evidence has been assembled during the effort reported herewith that support the contention that the spatial structures of ionospheric electron density observed by the ASTP MAO-89 Doppler Tracking Link are a real geophysical phenomenon and not an instrumentation artifact. The above can be stated based on several independent arguments: the physical plausibility of major structures observed by the ASTP Doppler Tracker (such as the Appleton anomaly); the consistency of the observations with the known properties of such ionospheric phenomena as medium-scale TIDs'; the similarity of the power spectra of the electron density irregularities as observed by the ASTP experiment and as measured by the AE satellite; and on other similar points.

We recommend that this research be carried further, with an additional effort devoted to the search for fully-probative corroborative evidence. The

new effort should be primarily directed at the comparison between the AE and ASTP data. Spectral indices should be computed and compared for AE and ASTP data sets of limited spatial and temporal extent (thus belonging to as small a fraction of an orbit as possible), all taken on 24 July 1975, the day when the ASTP data was collected. Additionally, the search for further corroborative evidence should include the examination of Total Electron Content (TEC) records of TEC links from synchronous satellite to ground, the review of the records of incoherent scatter radars and similar instruments and the review of other data sets containing observations that were performed in the volume and at the time of interest.

# APPENDIX A

## Observations of Ionospheric Wave Structures with Wave Length Less than 300 km, by the Apollo-Soyuz Satellite-to-Satellite Doppler Tracking Link.

# Observations of Ionospheric Wavestructures with Wavelengths Less Than 300 km by the Apollo-Soyuz Satellite-to-Satellite Doppler Tracking Link

by

Robert D. Estes and Mario D. Grossi

Harvard-Smithsonian Center for Astrophysics
Cambridge, Massachusetts 02138

## ABSTRACT

We analyze satellite-to-satellite Doppler tracking data taken during the 1975 Apollo-Soyuz mission for irregularities in electron density at an altitude of 220 km. The maximum entropy power spectrum of the electron density shows a peak corresponding to wavelengths of 250-300 km. A high pass filtering of the data reveals localized regions of fluctuations in the electron density having amplitudes of $3\text{-}5\times10^{9}$ $m^{-3}$ and wavelengths less than 300 km. Roughly half the localized wave structures, which are confined to dimensions of 1800 km or less (as seen by the satellites) are found to be associated with the larger crests of the geomagnetic anomaly in the southern (winter) hemisphere in the morning. The observed nighttime structures are also associated with local peaks in the electron density. We observe other wave structures at the day to night transition point, and we suggest atmospheric disturbances caused by the supersonic motion of the terminator as a possible generating mechanism. The amplitudes of the wave structures are roughly independent of the background density, in agreement with previous observations of TID. We conclude that our observations are consistent with their being medium-scale TID generated by atmospheric gravity waves.

## I. Introduction

Ionospheric electron density irregularities have been the subject of considerable research in recent years, since their causes have yet to be fully explained and their effects on communication, navigation, and geodetic systems can be seriously disruptive [Woodman and La Hoz, 1976]. Travelling ionospheric disturbances (TID) and the spread-F effect are among the important phenomena one might mention in this regard. Interest has centered on the role of atmospheric gravity waves as causative mechanisms for these phenomena [e.g., Hines, 1960; Davies and Jones, 1971; Rottger, 1973a,b, 1978; Francis, 1975, Booker, 1979]. Ionospheric irregularities have been studied by numerous techniques of ionospheric sounding and in-situ satellite probes.

The dual frequency satellite-to-satellite Doppler tracking system provides an alternative method of obtaining in a short time detailed information about the electron density distribution at a given altitude over a large portion of the globe. With this in mind, we have re-examined the satellite-to-satellite Doppler tracking data that were collected in the summer of 1975 by the MA-089 experiment conducted by our observatory on the occasion of the Apollo Soyuz Test Project (ASTP) [Weiffenbach,1977]. This experiment was the first ionospheric sounding ever performed between two satellites in low earth orbit, and to the best of our knowledge the data collected in this experiment remains the only data of its kind.

## II. Data Analysis and Discussion

### A. The Data Set

The ASTP data set consists of Doppler samples (each with 10 second integration time) collected with a mutually-phase-coherent pair of CW frequencies, 162 and 324 MHz, transmitted one-way from the transmitting to the receiving terminal (both at approximately 220 km height, with a link path of about 400 km). Data collection, which started at 1:01:56 GMT on July 24,1975 and continued for some 13 1/2 hours (approximately 9 revolutions), was distributed among all longtitudes and limited to a latitude span of ± 51.77° (orbital inclination). Full experimental details are given in Weiffenbach [1977] and Stiffler [1977].

### B. Differential Doppler Data Spectral Analysis

The raw data consists of the frequency shifts averaged over ten second intervals for the two different frequencies. The Nyquist period of 20 seconds corresponds to a wavelength of 156 km since the two satellite modules moved with a velocity of 7.8 km/sec.

The phase of the signal arriving at the receiving satellite after having traversed the distance $\Delta x$ through the ionospheric medium separating the two satellites is

$$\phi = \phi_0 + \frac{\omega}{c}\int_0^{\Delta x} n(x,\omega)\, dx \qquad (1)$$

where $\omega$ is the angular frequency of the signal and $n(x,\omega)$ is the index of refraction of the medium along the link path.

The index of refraction is given approximately by

$$n^2 = 1 - \frac{\omega_p^2}{\omega^2} \text{ or } n \simeq 1 - \frac{\omega_p^2}{2\omega^2} \qquad (2)$$

where the plasma frequency $\omega_p$ is defined (in Gaussian units) by the familiar expression

$$\omega_p^2 = \frac{4\pi N_e(x) e^2}{m} \qquad (3)$$

with $N_e$ the electron density and e and m the electron charge and mass, respectively, and $\omega_p \ll \omega$ .

$\phi$ is conveniently expressed as $\phi(\omega) = \phi_o + \frac{\omega}{c} \bar{n}(\omega) \Delta x$, where $\bar{n}(\omega)$ is the average index of refraction between the satellites. The observed frequency shift is given by

$$f_D(\omega) = \frac{1}{2\pi} \frac{d\phi}{dt} = \frac{1}{2\pi} \frac{\omega}{c} \left( \frac{d\bar{n}(\omega)}{dt} \Delta x + \bar{n}(\omega) \frac{d\Delta x}{dt} \right) \qquad (4)$$

and consists of two parts: the refractive part due to the changing electron density encountered along the orbit and the ordinary Doppler relative motion part.

In the dual frequency case one can eliminate the significant relative velocity term by obtaining the differential Doppler frequency

$$\delta f_D \equiv f_D(\omega_1) - \frac{\omega_1}{\omega_2} f_D(\omega_2) \qquad (5)$$

which turns out to be

$$\delta f_D = \frac{e}{mc\omega_1} \left[ \left( \frac{\omega_1}{\omega_2} \right)^2 - 1 \right] \Delta x \, v \frac{d\bar{N}_e}{dx} \qquad (6)$$

with v the satellite velocity and $\bar{N}$ the average electron density along the link path. The residual relative motion term has been dropped, since for our parameters it makes at most a one percent contribution when $\frac{1}{\bar{N}_e} \frac{d\bar{N}_e}{dx}$ is as low as $3 \times 10^{-8}$ cm$^{-1}$.

Thus the differential Doppler frequency is seen essentially to be proportional to the spatial derivative (along the direction of motion) of the average electron density between the two satellites.

To study the structure of the ionospheric variations we applied the maximum entropy method of spectral analysis [Ulryck,1975] to the differential Doppler data, using the Burg algorithm for estimating the prediction error coefficients.

The results of this spectral analysis of the data are shown in Figure 1, where the logarithm of the power spectral density is plotted versus frequency. Note in particular the peak seen in the frequency range .023-.035 Hz, which corresponds to a wavelength range of around 220-340 km, well within the range of horizontal wavelengths for gravity wave propagation at our altitude [Hines, 1960].

## C. Electron Density Analysis

In order to get a better feel for the physical significance of the data, we have integrated the differential Doppler data (with appropriate factor) to obtain the average electron density. This facilitates comparisons with previous observations as well. The value of the electron density is uncertain by an additive

constant, which we have chosen so as to confine the range of density values within well-known limits and to make the maximum and minimum values roughly coincide with those quoted in Weiffenbach [1977], namely a range between $3 \times 10^9$ $m^{-3}$ and $5 \times 10^{11}$ $m^{-3}$. Since the density must not become negative (or less than a few times $10^9$ $m^{-3}$ at 220 km) there is a natural lower limit to the value of the integration constant for a given set of data. While a change in the constant could shift the values up a few times $10^9$ $m^{-3}$, the qualitative behavior of the electron density should be well represented by our calculations.

We are particularly interested in wavestructures with wavelengths in the 200-300 km range, on the basis of the power spectrum of Figure 1. In order to determine the magnitude and the geographical and temporal distribution of possible periodic structures, we subjected the differential Doppler data to a high pass filter designed to pass frequencies greater than 1/40 $sec^{-1}$, or, equivalently, wavelengths less than 312 km. The filter used is a 101-term least-squares (Fourier) approximation to the filter with square transfer function. Convergence factors minimized the Gibbs phenomenon. For further details of the filter see Bloomfield [1976]. The results of a high pass filtering of the electron density are of course unaffected by the choice integration constant referred to above.

## 1. Total Electron Density Distribution

Figures 2 and 3 display the electron density (in units of $10^{11}$ el $m^{-3}$ ) seen as a function of time. The upper portions of the figures show the total data and the lower portions of the figures show the data after components with periods greater than 40 seconds have been removed. Time is given in UT seconds into July 24, 1975. The day/night transitions and equatorial crossings are marked in these figures. This is almost superfluous for the day/night transitions since the change in electron density is so dramatic. Daytime crossings of the equator are from south to north, nighttime crossings from north to south.

A prominent feature seen repeatedly in different revolutions is the geomagnetic anomaly or equatorial trough first observed by Appleton [1946] in which the electron-depleted magnetic equator is flanked by crests to the north and south. The marked north-south asymmetry, with the southern peak much higher and narrower than the northern peak, seen in Figure 3 is in good agreement with the distributions observed by Walker and Poon [1977] during summer soltice mornings for the same year (1975). This asymmetry has been explained by Bramley and Young [1968] as being due to the action of meridional winds. The displacement of the trough into the summer hemisphere, which can be seen in Figure 3, has been previously observed by Lyon [1963]. The correspondences between our data and these well-known phenomena give us confidence that our data provides an accurate

representation of at least the large-scale features of the electron density distribution encountered by the satellites. Other sharp peaks in the electron density can be seen near the day to night transitions in Figure 2. These are discussed below.

## 2. Electron Density Wavestructures

A number of wave-packet-like structures with relatively large amplitudes and confined to spatial regions of approximately 1800 km or less (along the satellite path) are seen at intervals in the filtered data displayed in the lower portions of Figures 2 and 3. Within these regions variations in the electron density with magnitudes up to $5 \times 10^9$ $m^{-3}$ and occurring over spatial dimensions of less than 312 km are superimposed on the longer wavelength variations.

For reference purposes several of the prominent short-wavelength structures visible in the lower sections of figures 2 and 3 have been labeled with a capital letter (A-M). The local times and at the center of these waveforms are also indicated in the figures. These prominent wave-structures can be broken into three general categories, as tabulated below.

| | | Event | Local Time | Geo. Longt. | Geo. Lat. | Mag. Inclination |
|---|---|---|---|---|---|---|
| | morning | A | 920 | 110° | 3°S | -19° |
| | | E | 920 | 42° | 4°S | -19° |
| | | G | 920 | 20° | 3°S | -22° |
| | | J | 855 | 356° | 5°S | -26° |
| | | K | 920 | 338° | 2°N | -9° |
| | | M | 825 | 303° | 15°S | -5° |
| | night | C | 300 | 9° | 52°S | -73° |
| | | F | 2200 | 215° | 2°S | -21° |
| | | I | 2130 | 195° | 5°S | -10° |
| | | L | 2200 | 158° | 16°S | -42° |
| day-to | night | B | 1930 | 255° | 31°N | 58° |
| | | D | 1940 | 238° | 26°N | 52° |
| | | H | 2035 | 174° | 21°N | 23° |

### 2(a) Morning Structures

The first category consists of the six daytime near-equatorial structures (A,E,G,J,K, and M). All of these structures are observed at local times between 0830 and 0930 hrs and are associated with large electron concentrations. They are observed repeatedly over a longitudinal range that stretches from the eastern coast of Africa to the middle of South America for the series E, G, J, K, and M. The most noteworthy feature about these structures is that they are all found within the larger, steeper anomaly crest south of the magnetic equator. In the

revolution which saw the least pronounced asymmetry (around time 12000 seconds in Figure 2) there is only a hint of a distinct localized wave structure in the filtered data.

Steep vertical gradients are evidently associated with the sharp southern peaks, based on the observations reported by Lyon [1963] in which it was found that, although the maximum electron density was on the winter side, the height at which the local maximum occurred was considerably greater on the summer side. The role of sharp vertical gradients of the electron density in enhancing the ionospheric response to atmospheric gravity waves is well known (See, for example, Hooke [1970]). The linearized continuity equation for electrons in the presence of an atmospheric wave with associated fluid velocity $\vec{u}$, where we restrict electron motion to be along the magnetic field lines, yields the following expression for the ratio of the perturbation of the electron density $N_e$ to the unperturbed electron density $N_{eo}$ at a height z:

$$\frac{N_e}{N_{eo}} = \vec{u} \cdot \hat{b} \left\{ \vec{k} \cdot \hat{b} + i \hat{z} \cdot \hat{b} \left[ \frac{1}{2H} + \frac{1}{N_{eo}} \frac{dN_{eo}}{dz} \right] \right\} \qquad (7)$$

where $\vec{u}$ is of the form

$$\vec{u} = \vec{u}_o \exp (z/2H) \exp (i[\omega t - \vec{k} \cdot \vec{r}]) \qquad (8)$$

with $\omega$ the angular frequency of the gravity wave, $\vec{k}$ the wave vector of the gravity wave, $\hat{b}$ the unit vector along the magnetic field line, $\hat{z}$ the unit vector in the vertical direction, and H the neutral atmospheric scale height.

From equation (7) it is clear that a large value of $\frac{1}{N_{eo}} \frac{dN_{eo}}{dz}$ can lead to significant fluctuations even if the wave vector is nearly perpendicular to the magnetic field line ($\hat{k} \cdot \hat{b}$ small) and if the dip angle is small, i.e., if $\hat{z} \cdot \hat{b}$ is small, as it is near the equator. The observed fluctuation levels for the morning events are all less than 1%.

Our Doppler tracking data shares one disadvantage with in-situ measurements: it cannot be used to determine the velocity of any ionic structures encountered, so that without independent observations of another type it is impossible to definitively identify TID. In certain respects, including their wavelengths and position in the equatorial region, the structures do suggest TID, however. So far as we know TID have not been connected with the steep anomaly peak before, but it would be of interest to see if such a relationship exists in other data.

Rottger [1973b] did in fact observe TID precisely in the region of the southern anomaly crest in data from August-September, 1969, but he concluded that a connection with the geomagnetic anomaly was ruled by the observed diurnal frequency distribution of TID, which had clear peaks in the

morning (600-930) and evening (1700-2100) hours, reasoning that the anomaly was most pronounced in the early afternoon. It is not apparent, however, whether Rottger considered the possibility that steep morning gradients in electron density could have been decisive.

2(b) Nighttime Structures

The second category consists of the nighttime structures: the three lower latitude southern hemispheric structures (F,I, and L), all of which occur at around 2130 to 2200 local time, and structure C , the post-midnight structure (local time 0300 hrs) seen at 46 S. These structures are associated with nighttime peaks in the electron density. In the case of structures F, I, and L these peaks may be the residual southern hemispheric anomaly crests. Event C lies near the latitudinal limit of the satellite orbit, and the associated electron density peak must therefore have some other explanation than the Appleton anomaly. The two structures designated F and I in Figure 2 may in fact be the same structure seen in two successive revolutions since both events are confined to a reasonably small area a few degrees south of the equator for longtitudes around 200 east.

While these nighttime peaks are small compared to the large concentrations observed in the Appleton anomaly daytime peaks, for example, they are not small compared to the local background density, i.e. $\Delta n/n$ is far from small. We cannot be precise about this ratio because of the uncertainty introduced by our integration constant. It seems clear, however, that the ratio is quite large and that the vertical logarithmic derivative of the electron density is possibly large also, which would be important to the ionospheric response to atmospheric waves , even though the linear equation (7) is no longer applicable.

The nighttime equatorial region observations of Rottger [1973,1978] may be relevant to our own. He saw quasi-periodic structures of spread-F irregularities in the nighttime equatorial regions that moved in an eastward direction and had wavelengths in the 200-600 km range. Rottger [1978] attributed their growth to the spatial resonance mechanism [Whitehead,1971; Klostermeyer,1978] which occurs when the phase velocity of the gravity wave equals the ionospheric plasma drift velocity. This mechanism is found by Rottger [1978] to be most likely between 2100 and 2300 hrs local time, which is consistent with our observed nighttime equatorial structures F, I, and L, all of which occur between 2100 and 2200 hrs.

2(c) Day-to-night Transition Structures

The third category includes the three structures observed at the day to night transition, which occurs (at 220 km) around 1930-2000hrs local time. These are the structures designated B, D, and H in the figures. The sharp peaks in the total electron

density associated with events B and D seem noteworthy. To us, they suggest the sharp buildup in front of a shock wave, and we are reminded that Cole [1974] and Beer [1973] have proposed that a shock wave generated by the supersonic motion of the terminator with respect to atmospheric winds could be a source of TID or irregularities associated with the spread-F phenomenon.

TID generated by the supersonic motion of the moon's shadow across the earth have probably been observed [Davis and Da Rosa, 1971; Arendt, 1971; Chimonas and Hines, 1971]. Raitt and Clark [1973] reported they found possible evidence for dawn supersonic terminator generation of gravity waves in Langmuir probe data taken by the ESRO-1A satellite, but their evidence was less direct than our own (though based on much more data). In the absence of more data we merely note the shockwave mechanism as an interesting hypothesis to explain these observations.

2(d) General Observations

An interesting general observation about the data is that the maximum amplitudes of the localized wave packets observed in the filtered data are relatively independent of the total electron density where they occur, remaining approximately the same ($3\text{-}5 \times 10^9$ $m^{-3}$) while the background density varies by a factor of at least ten and perhaps one hundred. This would seem to exclude as the generating mechanism those factors that are associated with the ionized portion of the upper atmosphere, at satellite heights. We note that this observation is in agreement with that made by Titheridge [1968] with respect to TID in his comprehensive study of data taken over a period of several years. He found the absolute value of the changes in electron content produced by equatorial TID day and night was independent of the background electron content.

Nine of the thirteen prominent structures designated by capital letters in Figures 2 and 3 occur in regions for which the magnitude of the magnetic inclination is less than thirty degrees. TID generated by atmospheric gravity waves are known commonly to occur in the equatorial regions [Booker,1979; Nagpal et al.(1973); Rottger, 1973a,b; Sterling, et al.,1971]. The observed wavelengths, which are only order of magnitude observations, since we do not know the angle between the wavefronts and the satellite paths, are consistent with those previously observed for medium-scale TID.

III. Conclusions

In conclusion, then, we can say that the characteristics of the wave structures that apppear in our analysis are consistent with their being medium-scale TID generated by atmospheric gravity waves. While all of the observed structures are found to be associated with local peaks in the electron density, not all electron density peaks have wave structures associated with them.

For example the nighttime peak around 15000 sec in Figure 3 does not. The factors that determine when the wave structures occur remain unknown, though we have discussed the problem in general terms, pointing out the possible importance of steep vertical gradients of electron density in the morning Appleton anomaly crest and proposing an atmospheric shock wave generated by supersonic terminator motion as the generating mechanism in the case of the day-to-night transition structures.

All of the above results were obtained with a data sample that was collected in only 13 1/2 hours. The Doppler tracking method of ionospheric sounding, with the Doppler link established between two satellites in low altitude Earth orbit has proven to be a powerful tool that adds substantially to earth-based ionospheric observations. It would seem advisable to repeat the experiment with a much longer duration of the data collection in order to investigate the frequency, distribution, and seasonal variations of these phenomena and to learn more about their connection with other ionospheric phenomena and about their causative mechanisms.

## IV. Acknowledgments

We wish to acknowledge a stimulating discussion with Dr. Stanley Gross and Mr. Cliff Friedman of the Polytechnic Institute of New York. We are grateful to Dr. Gross for suggesting the application of the maximum entropy method of spectral analysis.

This work was supported in part by NASA Grant NAS 5-36 and Polytechnic Institute of New York Subcontract 23719 (NASA Grant NASW-51)

References

Appleton, E.V. (1946), Two anomalies in the ionosphere, Nature, vol.157, p.691
Arendt, P.R. (1971) Ionosphere-gravity wave interactions during the March 7, 1970, solar eclipse, J. Geophys. Res., vol.76, p.4695
Beer, T. (1973) Supersonic generation of atmospheric waves, Nature, vol.242, p.34
Bloomfield, P. (1976), Fourier Analysis of Time Series: An Introduction, pp.129-136, John Wiley and Sons, New York
Booker, H.G. (1979), The role of acoustic gravity waves in the generation of spread-F and ionospheric scintillation, Journal of Atmospheric and Terrestrial Physics, vol.41, p.501
Bramley, E.N. and M. Young [1968] Winds and electromagnetic drifts in the equatorial F2-region, J. of Atm. Terr. Phys., vol.30, p.99
Chimonas, G. and C.O. Hines (1971) Atmospheric gravity waves induced by a solar eclipse, 2, J. Geophys. Res., vol.76, p.7003
Cole, K.D. (1974) Energetics of and a source of energy for equatorial spread-f events, J. of Atm. Terr. Phys., vol.36, p.1099
Davies,K. and J.E. Jones (1971) Three-dimensional observations of travelling ionospheric distrubances, J. of Atm. Terr. Phys., vol.33, p.39
Davis, M.J. and A.V. Da Rosa (1970) Possible detection of atmospheric gravity waves generated by the solar eclipse, Nature, vol.226, p.1123
Francis, S. (1975), Global propagation of atmospheric gravity waves: a review, J. of Atm. Terr. Pnys., vol.37, p.1011
Hines, C.O. (1960), Internal atmospheric gravity waves at ionospheric heights, Can. J. Phys., vol.38, p.1441
Hooke, W.H. (1970) The ionospheric response to internal gravity waves: 1. The F2 region response, J. Geophys. Res., vol.75, p.5535
Klostermeyer, J. (1978), Nonlinear investigation of the spatial resonance effect in the nighttime equatorial F region, J. of Geophys. Res., vol.83, p.3753
Lyon, A.J. (1963) The Physics of the Atmosphere, Physical Soc. London, p.88
Nagpal, O.P., A.B. Gupta, and C.S.G.K. Setty (1973) Some studies of atmospheric gravity waves at equatorial and temperate latitudes, Ann. Geophys., vol.29, p.293
Raitt, W.J. and D.H. Clark (1973) Wave-like disturbances in the ionosphere, Nature, vol.243, p.508
Rottger, J. (1973a) Wave-like structures of large-scale equatorial spread-F irregularities, J. of Atm. Terr. Phys., vol.35, p.1195
Rottger, J. (1973b) Some properties of large-scale equatorial spread-F irregularities interpreted by influences of atmospheric gravity waves, Zeit. Geophysik, vol.39, p.799
Rottger, J. (1978) Drifting patches of equatorial spread-F irregularities -- experimental support for the spatial

resonance mechanism in the ionosphere, J. of Atm. Terr. Phys., vol.40, p.1103

Sterling, D.L., D.H. Hooke, and R. Cohen (1971) Travelling Ionospheric Disturbances Observed at the Magnetic Equator, J. of Geophys. Res., vol.76, p.3777

Stiffler, J.J., A.C. Berg, and D.G. Young (1977) Phase-coherent dual-frequency link for high precision Doppler tracking between spacecraft, Space Sci. Instr., vol.3, p.3

Titheridge, J.E. (1968), Periodic Disturbances in the Ionosphere, Journal of Geophysical Research, Space Physics, vol.73, p.243

Ulryck, T.J. and T.N. Bishop (1975), Maximum entropy spectral analysis and autoregressive decomposition, Rev. Geophys. Sp. Phys., 13, 183-200.

Walker, G.O. and C.B. Poon (1977), The early morning development and the evening decay of electron content latitude profiles at low latitudes and their dependence upon solar declination, J. of Atm. Terr. Phys., vol.39, p.1145

Weiffenbach, G.C., M.D. Grossi, and P.W. Shores (1977), Doppler tracking experiment MA-089, Summary Science Report, Apollo-Soyuz Test Project, Volume I, pp.137-175.

Whitehead, J.D.(1971)Ionization disturbances caused by gravity waves in the presence of an electrostatic field and background wind, J. Geophys. Res. , vol.76, p.238

Woodman, R.F. and C. La Hoz (1976), Radar Observations of F Region Equatorial Irregularities, Journal of Geophysical Research, vol.81, p.5447

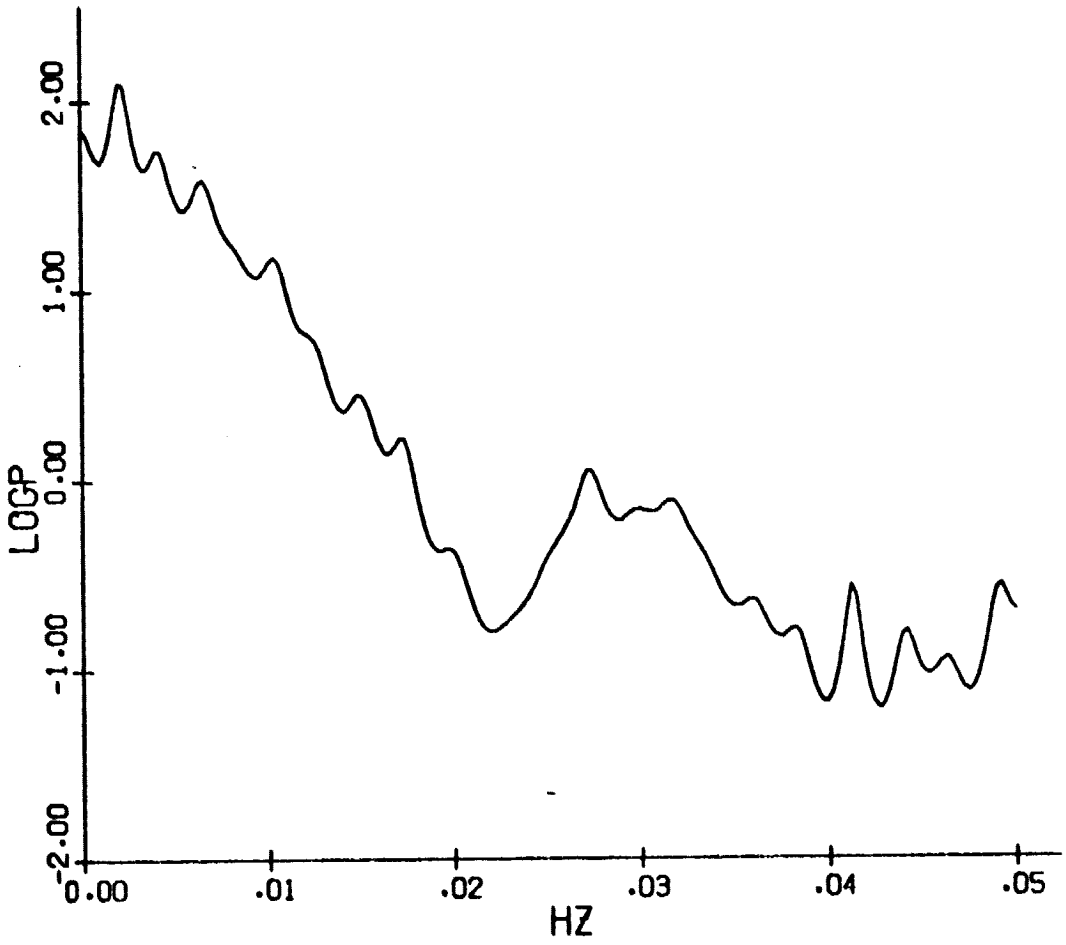


Figure 1. Logarithm of power spectral density (arbitrary scale) of differential Doppler data obtained by maximum entrophy method plotted versus frequency. 0.01 Hz corresponds to a wavelength of 780 km.

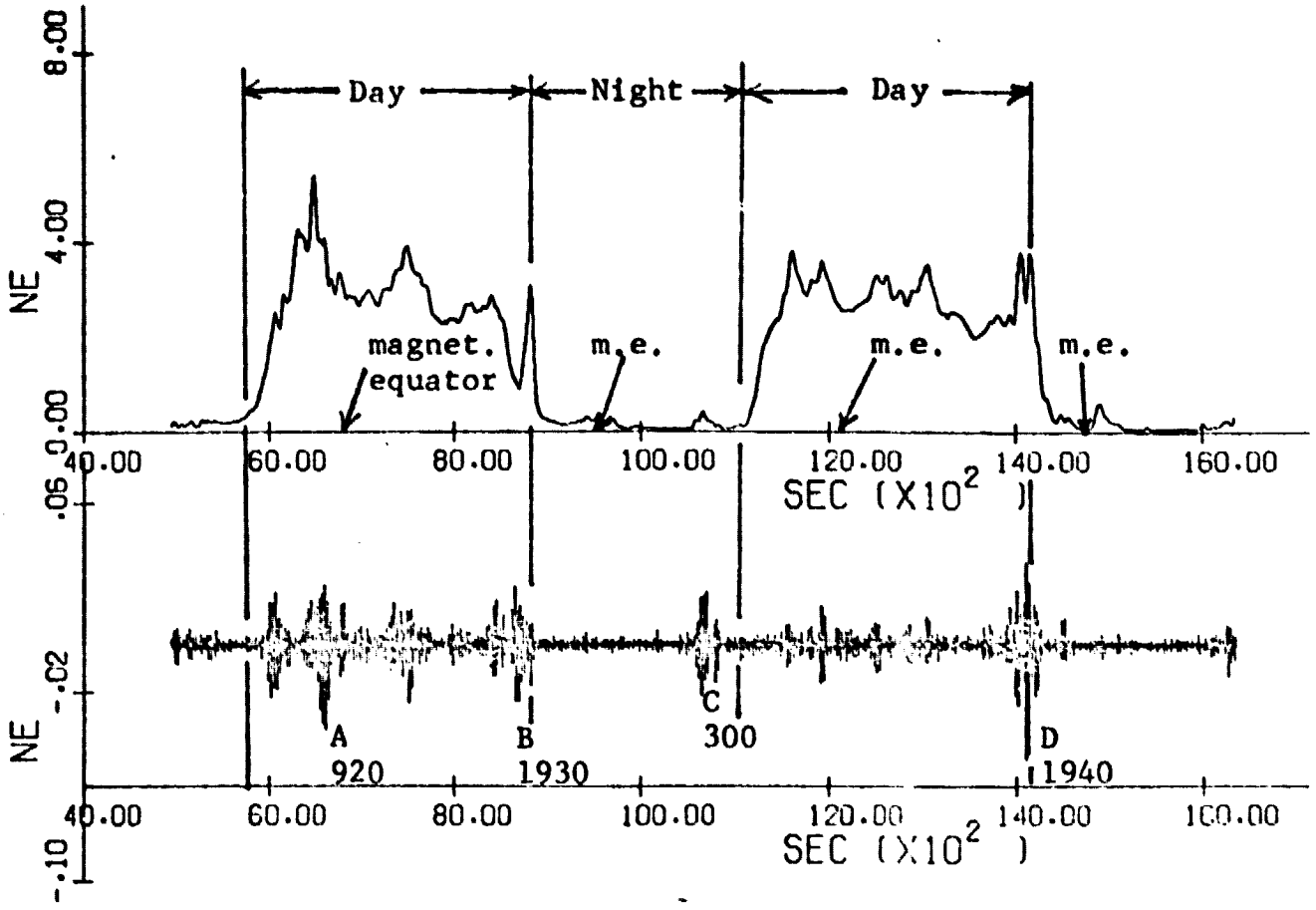


Figure 2. Upper: average electron density in units of $10^{11}$ m$^{-3}$ versus time (ut seconds), July 24, 1975.

Lower: same data with wavelengths less than 312 km removed; local time indicated for designated events.

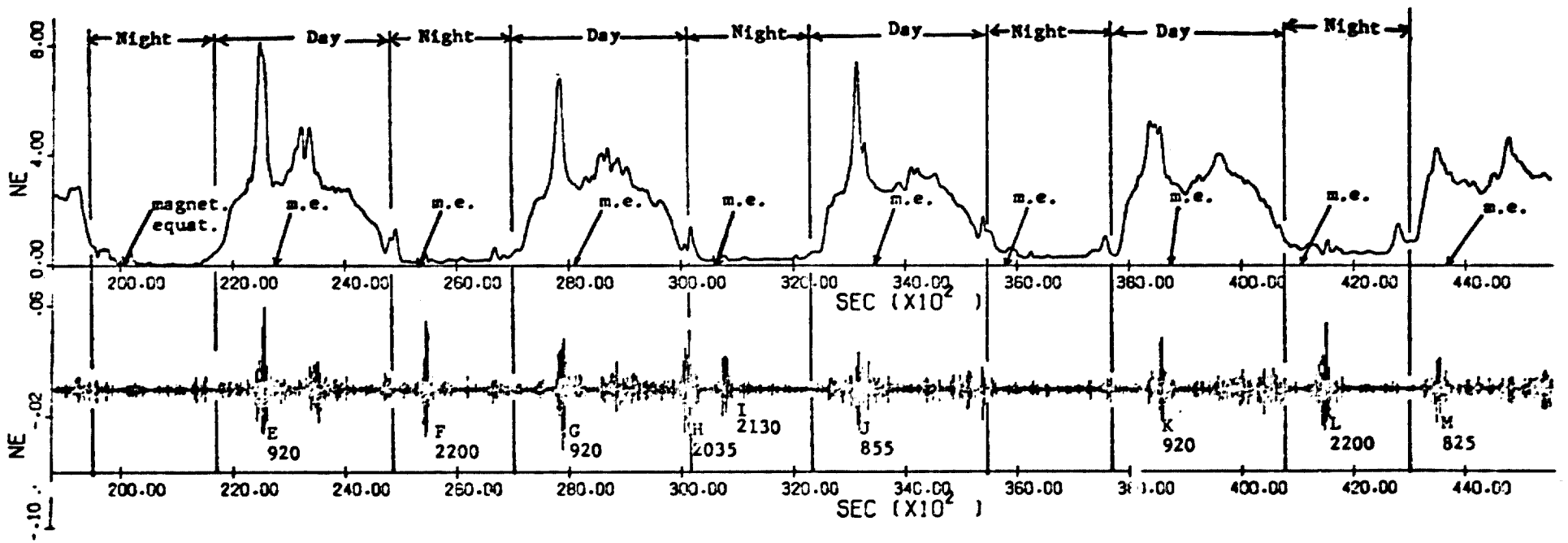


Figure 3. Upper: average electron density in units of $10^{11}$ $m^{-3}$ versus time (ut seconds), July 24, 1975.

Lower: same data with wavelengths greater than 312 km removed; local time indicated for designated events.